Advanced Physical Research
Vol.7, No.3, 2025, pp.334-349
https://doi.org/10.62476/apr.73334

# THE PHYSICAL PROPERTIES OF THE PEROVSKITE COMPOUND STRONTIUM ZICONATE WERE CALCULATED BASED ON DENSITY FUNCTIONAL THEORY (DFT) METHODS

**Amena Abdulqader Mohammed***, **Abdulhadi Mirdan Ghaleb**

Department of Physics, College of Sciences, University of Kirkuk, Kirkuk, Iraq

**Abstract.** In this study, the structural, electronic, optical, Mulliken charge distribution, and bond length characteristics of cubic perovskite $SrZrO_3$ are systematically investigated using Density Functional Theory (DFT) with Local Density Approximation (LDA), Generalized Gradient Approximation (GGA), and meta-GGA (M-GGA) exchange–correlation functionals. The computed results are critically compared with available experimental data. Structural optimization yields lattice parameters of 4.117 Å (LDA), 4.186 Å (GGA), and 4.130 Å (M-GGA), relative to the experimental value of 4.084 Å. These results indicate that LDA slightly underestimates the lattice constant, while GGA overestimates it; M-GGA provides the closest agreement due to its improved treatment of exchange–correlation interactions. Electronic structure calculations reveal functional-dependent trends in band gaps. The LDA (3.108 eV) and GGA (3.130 eV) approximations significantly underestimate the experimental band gap, whereas M-GGA (3.963 eV) provides values in much closer agreement. $SrZrO_3$ is thus confirmed as a wide-band-gap semiconductor, with an energy gap ranging from ∼3.2 eV to ∼4.0 eV. Analysis of the total density of states (TDOS) reveals strong Zr–O orbital hybridization: the O 2p orbitals contribute predominantly to the valence band, while the Zr 4d orbitals dominate the conduction band. The optical response, including the dielectric function and absorption coefficient, further reflects the influence of functional choice. LDA and GGA predict red-shifted absorption edges due to band gap underestimation, whereas M-GGA more accurately reproduces the experimental optical onset at approximately 3.2 eV. Despite quantitative differences, all functionals capture the dominant optical features of $SrZrO_3$.Finally, Mulliken population analysis, bond length evaluation, and charge distribution calculations are performed within the same approximations, offering complementary insights into the bonding characteristics and electronic environment of $SrZrO_3$.

**Keywords**: DFT, (LDA, GGA, and M-GGA), physical properties of $SrZrO_3$.
***Corresponding author:** Amena Abdulqader Mohammed, Department of Physics, College of Sciences, University of Kirkuk, Kirkuk, Iraq, e-mail: *abdlhadik@uokirkuk.edu.iq, scpm23012@uokirkuk.edu.iq*
*Received: 1 August 2025; Revised: 30 August 2025; Accepted: 1 September 2025; Published: 16 October 2025.*

## 1 Introduction

The general chemical formula of perovskites is represented as $ABO_3$, where their structural flexibility enables the development of a wide variety of functional systems. Among their remarkable physical properties, ferroelectricity and piezoelectricity are of particular significance, providing these materials with distinct advantages over conventional alternatives. Due to these properties, perovskite oxides have been widely adopted in various technological applications, including high-temperature oxygen and hydrogen sensors, solid oxide fuel cells, data storage devices (e.g., hard drives), and light-emitting components, such as bright blue emitters. Furthermore, their use extends to the fabrication of capacitors and other multifunctional electronic

devices (Davies et al., 1999; Fukatsu et al., 1995; Yajima et al., 1992; Yu et al., 2004; Souptel et al., 2002; Muscat et al., 2001). Within this class, strontium zirconate ($SrZrO_3$) represents one of the most important members of the zirconate perovskite family, primarily due to its exceptionally high proton conductivity at elevated temperatures, making it a promising candidate for next-generation electrochemical and energy conversion technologies (Sambrano et al., 2005).

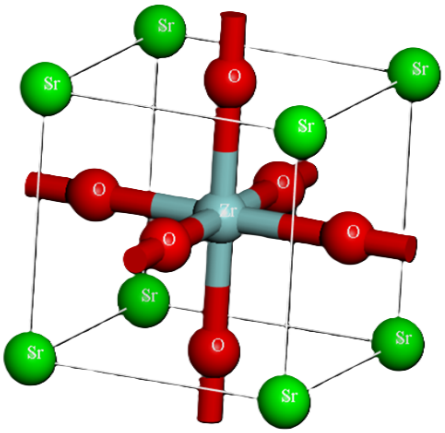


**Figure 1:** The cubic structure of ($SrZrO_3$) in the unit cell.

Figure 1 illustrates the unit cell of the cubic perovskite $SrZrO_3$ crystal structure (space group $Pm\bar{3}m$). In this configuration, Sr atoms occupy the corners of the unit cell and are positioned nearest to the O atoms, while the Zr atom resides at the center of the unit cell, being coordinated with six surrounding oxygen atoms in an octahedral arrangement. The oxygen atoms are located on the faces of the unit cell, each bonded to two Zr atoms. Owing to its high relative permittivity (dielectric constant), high breakdown strength, and low leakage current, $SrZrO_3$ is considered a promising material for high-voltage devices and capacitor-based applications (Sambrano et al., 2007; Vali, 2008). Study the phase transition of $SrZrO_3$ using the artist and powder neutron diffraction (PND) techniques (Galicka-Fau et al., 2008). Their results demonstrated that $SrZrO_3$ undergoes successive phase transitions from the orthorhombic Pnma phase to orthorhombic Cmcm at approximately 970 K, 1100 K, and 1400 K, respectively. Upon further heating, the material transforms into a tetragonal phase (I4/mcm) before stabilizing in the cubic phase ($Pm\bar{3}m$). At extremely high temperatures (around 2920 K), $SrZrO_3$ reaches its melting point and transitions into the liquid phase (Tsai & Teng, 2008). There are also several studies conducted using both the approximations (LDA and GGA) around the cubic (Ghaleb & Ahmed, 2022; Ghaleb et al., 2022). In addition to experimental studies, first-principles calculations have been employed to investigate the magnetic, electronic, optical, and structural properties of $SrZrO_3$, providing valuable insight into its potential applications in advanced functional devices (Feng et al., 2008; Marana et al., 2008; Park et al., 2006; Wu et al., 2008; Shende et al., 2001). The properties of $SrZrO_3$ have been extensively investigated by various researchers using different computational approaches. Techniques such as the full-potential linearized augmented plane wave (FPLAPW) method, density functional theory (DFT), linear combination of atomic orbitals (LCAO), and plane-wave (PW) analysis have been applied to explore its electronic structure and optically related characteristics (Iwahara et al., 1993; Colomban, 1992). Among these, the CASTEP code has proven particularly valuable, as it enables the calculation of ground-state energy, band structures, density of states (DOS), phonon dispersion, and elastic constants, thereby providing detailed insights into the material's behavior at the atomic level. CASTEP offers significant advantages for studying $SrZrO_3$, especially due to its effective treatment of complex crystal structures using periodic boundary conditions. In such simulations, the exchange–correlation functional is typically described within the generalized

gradient approximation (GGA) or the local density approximation (LDA), depending on the required balance between accuracy and computational cost. For the cubic phase of $SrZrO_3$, the Perdew–Burke–Ernzerhof (PBE) functional within (GGA), and in some cases the (m-GGA), is commonly employed because it provides reliable predictions of both structural and dynamical properties of oxide materials (Perdew et al., 1996).

## 2 Computational method

In this study, first-principles density functional theory (DFT) calculations were performed within the plane-wave pseudopotential framework using the CASTEP package (Materials Studio 2020) to investigate the structural and electronic properties of cubic perovskite $SrZrO_3$. Three exchange–correlation functionals were systematically examined to evaluate their performance: the Local Density Approximation (LDA), the Generalized Gradient Approximation in the Perdew–Burke–Ernzerhof form (GGA-PBE), and the meta-Generalized Gradient Approximation (SCAN). At 0 K, $SrZrO_3$ crystallizes in the ideal cubic perovskite structure with the $Pm\bar{3}m$ space group (No. 221). At ambient temperature, the material maintains this cubic symmetry, with Zr atoms occupying the body-centered position (0.5, 0.5, 0.5), Sr atoms located at the origin (0.0, 0.0, 0.0), and O atoms residing at the face-centered positions (0.5, 0.5, 0) and (0.5, 0, 0.5), forming a network of oxygen octahedra around the central Zr cation. To ensure accurate representation of the electronic structure, the following valence electron configurations were considered: $O(2s^22p^6), Zr(4s^24p^64d^25s^2), and Sr(4s^24p^65s^2)$. A plane-wave cutoff energy of 600 eV was employed, as convergence tests confirmed that increasing the cutoff further altered the total energy by less than 1 meV/atom. For Brillouin zone sampling, a dense $12\times12\times12$ Monkhorst–Pack k-point mesh was adopted. Geometry optimization was carried out using the Broyden–Fletcher–Goldfarb–Shanno (BFGS) minimization scheme(Ling et al., 2002). The optimized lattice parameters and total energies obtained from LDA, GGA-PBE, and SCAN were compared to identify systematic trends and deviations. Furthermore, the influence of each functional on the electronic properties, including bandgap values and the relative positions of the valence band maximum (VBM) and conduction band minimum (CBM), was thoroughly analyzed.

## 3 Results and Discussion

### 3.1 Geometry of Optimized Structure

The cubic phase of $SrZrO_3$ crystallizes in the $Pm\bar{3}m$ space group (No. 221) with an initial lattice parameter of a = b = c = 4.084Å(Celik & Cabuk, 2013), which lies between previously reported experimental values of 4.152 Å (Kennedy et al., 1999), and 4.109 Å(Smith & Welch, 1960). Lattice constants determined experimentally are also consistent with theoretical predictions using LDA and GGA, which report 4.095 (Mete et al., 2003). The lattice parameters follow the cubic symmetry condition, $\alpha = \beta = \gamma = 90°$, and the atomic positions and lattice constants were fully optimized by minimizing the total energy under zero external stress. The optimized unit cell structure is illustrated in Figure 1, consisting of five atoms: Zr occupies the body center, Sr is located at the corners, and three oxygen atoms reside at the face-centered positions. Table 1 presents the calculated lattice parameters of cubic $SrZrO_3$ obtained using three DFT approximations: Local Density Approximation (LDA), Generalized Gradient Approximation (GGA), and meta-GGA (m-GGA). The optimized lattice constants obtained in this work are 4.117 Å (LDA), 4.186 Å (GGA), and 4.130 Å (m-GGA). Corresponding unit cell volumes are $69.830Å^3$(LDA), $73.373Å^3$(GGA), and$70.444Å^3$ (m-GGA). These values closely approach the experimental volumes of $71.576Å^3$ and $69.375Å^3$, confirming the reliability and accuracy of the

**Table 1:** Using LDA, GGA, and M-GGA, the structural parameter of the $SrZrO_3$ cube phase was determined and compared with experimental data (Kennedy et al., 1999; Smith & Welch, 1960)

| Phase | Approach | $a^\circ = b^\circ = c$ (Å) | $V$ (Å$^3$) | Reference |
|---|---|---|---|---|
| $SrZrO_3$ | LDA | 4.117 | 69.830 | Present work |
| | GGA | 4.186 | 73.373 | |
| | m-GGA | 4.130 | 70.444 | |
| | LDA, GGA | 4.095 | 68.669 | (Mete et al., 2003) |
| | Experiment | 4.152 | 71.576 | (Kennedy et al., 1999) |
| | Experiment | 4.109 | 69.375 | (Smith & Welch, 1960) |

DFT-based calculations. The volumetric agreement between theory and experiment provides further evidence of the predictive accuracy of first-principles methods for $SrZrO_3$.

### 3.2 Electronic Structure

Density functional theory (DFT) is a widely used quantum mechanical method for investigating the electronic properties of materials. Within the Kohn-Sham framework, DFT reduces the complex many-body electron problem to a set of single-particle equations, where the exchange–correlation functional plays a critical role in determining the accuracy of the calculated electronic structure(Kohn & Sham, 1965). Understanding the electronic band structure is particularly important for semiconductors and insulators, as the nature of the band gap—whether direct or indirect—strongly influences their optoelectronic performance. For instance, materials with a direct band gap, where the valence band maximum (VBM) and conduction band minimum (CBM) occur at the same k-point (typically the G-point), are especially valuable in optoelectronic applications such as light-emitting diodes (LEDs), laser diodes, and photovoltaic cells. The choice of exchange–correlation functional significantly affects the predicted electronic properties. In the Local Density Approximation (LDA), the exchange–correlation energy depends solely on the local electron density. While computationally efficient, LDA often underestimates band gaps due to its tendency to overbind electrons(Perdew & Zunger, 1981). To address this limitation, the Generalized Gradient Approximation (GGA), which incorporates the gradient of the electron density, provides a more accurate description for inhomogeneous systems. Among GGA functionals, the Perdew–Burke–Ernzerhof (PBE) formulation has been widely adopted, as it generally yields improved predictions of lattice parameters and electronic structures compared to LDA, although it still systematically underestimates band gaps (Perdew, 1997). Beyond the density and its gradient, meta-GGA (m-GGA) functionals incorporate the kinetic energy density, thereby providing an additional level of approximation. Among these, the modified Becke–Johnson (mBJ) potential has attracted considerable attention due to its ability to predict band gaps with values much closer to experimental results (Tran & Blaha, 2009). A direct band gap occurs when both the valence band maximum (VBM) and conduction band minimum (CBM) lie at the Γ-point (the center of the Brillouin zone), a characteristic essential for understanding optical transitions and evaluating optoelectronic performance. For perovskite oxides such as $SrZrO_3$, reported band gap characteristics vary depending on the exchange–correlation functional employed. While LDA and GGA calculations typically predict an indirect band gap, the application of the mBJ potential often results in a direct G–G transition, thereby enhancing the material's suitability for optoelectronic applications in practice. The ground-state electron density is obtained through self-consistent field (SCF) iterations, followed by non-self-consistent band structure calculations along high-symmetry directions of the Brillouin zone. For $SrZrO_3$, DFT studies generally report a band gap of ∼3.8 eV with LDA, 4.0–4.2 eV with GGA, and 5.0–5.3 eV with m-GGA (notably with mBJ), which frequently accounts for the indirect-to-direct gap correction(Zhao & Vanderbilt, 2002). According to Table 2, the calculated band gaps of cubic $SrZrO_3$ in this work were 3.108 eV (LDA), 3.130 eV (GGA), and 3.963 eV (m-GGA). All

three approximations overestimate the experimental band gap of 3.75 eV, although the relative trend is consistent (LDA < GGA < m-GGA) (Moreira et al., 2009). This systematic progression highlights the increasing accuracy of higher-level functionals in capturing the electronic structure of $SrZrO_3$.

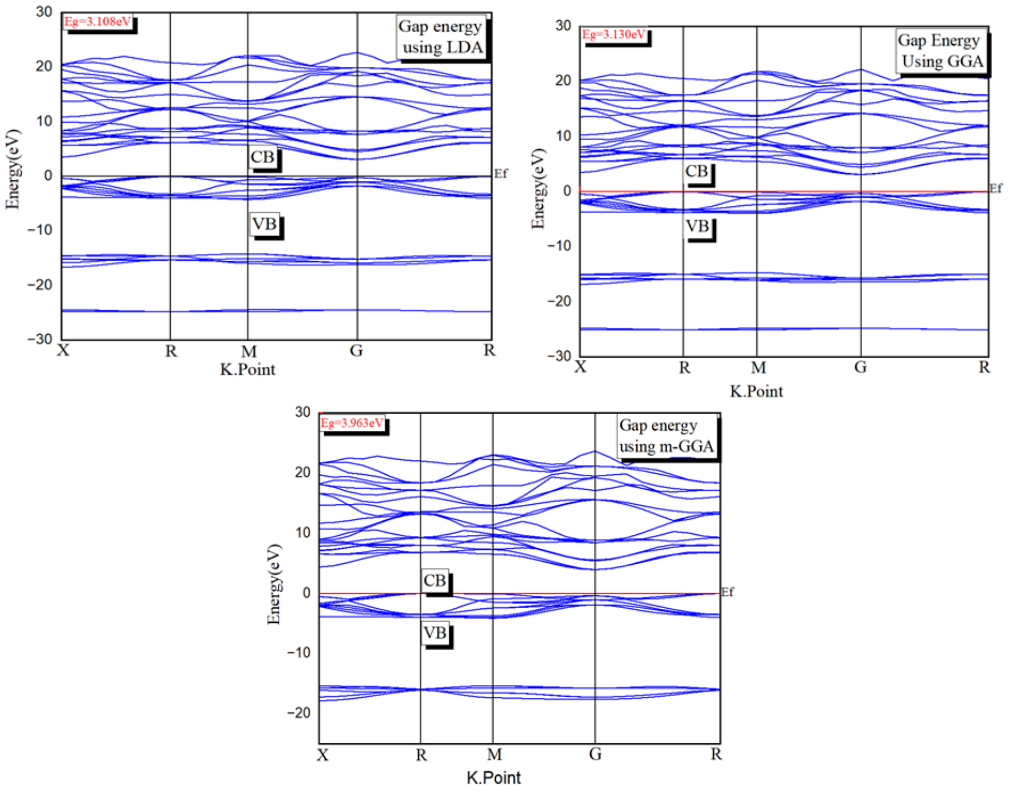


**Figure 2:** Band structures of the (SrZrO3) phase using the LDA, GGA, and m-GGA methods.

**Table 2:** The table presents the calculated energy band gap ($E_g$) of $SrZrO_3$, obtained using different exchange–correlation functionals, including LDA, GGA, and m-GGA.

| Phase | Approach | $E_g$ (eV) | Reference |
|---|---|---|---|
| $SrZrO_3$ | LDA | 3.108 | Present work |
| | GGA | 3.130 | |
| | M-GGA | 3.963 | |
| | Experiment | 3.75 | (Shein et al., 2007) |

## 3.3 Density of States

One of the most significant outcomes of density functional theory (DFT) calculations of electronic structures is the total density of states (TDOS). The TDOS provides information on the number of electronic states available at each energy level, making it an essential tool for understanding the electrical, optical, and magnetic properties of materials. From TDOS analysis, key characteristics such as the band gap, Fermi energy, valence band maximum (VBM), and conduction band minimum (CBM) can be extracted. Within DFT, the complex many-body problem of interacting electrons is reduced via the Kohn–Sham formalism to a system of non-interacting electrons moving in an effective potential. The band structure, from which the TDOS is derived, is determined from the eigenvalues of these equations. By summing the contributions of electronic states across all atoms and k-points in the unit cell, the TDOS of a material is obtained. The density of states (DOS) analysis is a powerful approach for eluci-

dating the bonding nature and electronic transitions in cubic strontium zirconate ($SrZrO_3$), a wide band-gap perovskite oxide. Using DFT, the TDOS of $SrZrO_3$ can be determined with high accuracy, enabling investigation of its semiconducting properties and potential applications in dielectric and optoelectronic devices. In this work, the DOS of cubic $SrZrO_3$ (space group $Pm\bar{3}m$) was calculated using the CASTEP code within the plane-wave pseudopotential framework. The exchange–correlation functional was treated primarily with the Perdew–Burke–Ernzerhof (PBE) formulation of the generalized gradient approximation (GGA), while comparative calculations were also performed using the local density approximation (LDA) and the (m-GGA). Before DOS calculations, the crystal geometry was fully optimized, and convergence was ensured using a dense Monkhorst–Pack k-point mesh along with a plane-wave cutoff energy of 600 eV. The computed TDOS confirms that $SrZrO_3$ is a wide band-gap semiconductor. The valence band is dominated by strong hybridization between O 2p states and Zr 4d orbitals, indicating covalent bonding interactions, while Sr contributes minimally near the Fermi level due to its predominantly ionic role in the lattice. The conduction band is primarily composed of unoccupied Zr 4d states. This electronic distribution highlights the mixed ionic–covalent nature of bonding in $SrZrO_3$. The calculated band gap is dependent on the chosen exchange–correlation functional: GGA predicts ∼3.2 eV, LDA underestimates the value at ∼2.7 eV, and m-GGA increases the estimate to ∼5.0–5.3 eV, closer to the experimental band gap (Chakraborti et al., 2016). Although DFT is known to underestimate band gaps in general, the DOS analysis presented here provides valuable insights into the electronic structure of $SrZrO_3$. In particular, the strong O 2p–Zr 4d interactions and the wide band-gap character suggest promising applications in high-temperature, dielectric, and insulating technologies. These findings underscore the importance of combining theoretical predictions with experimental validation for the further development of $SrZrO_3$ as a functional oxide material.

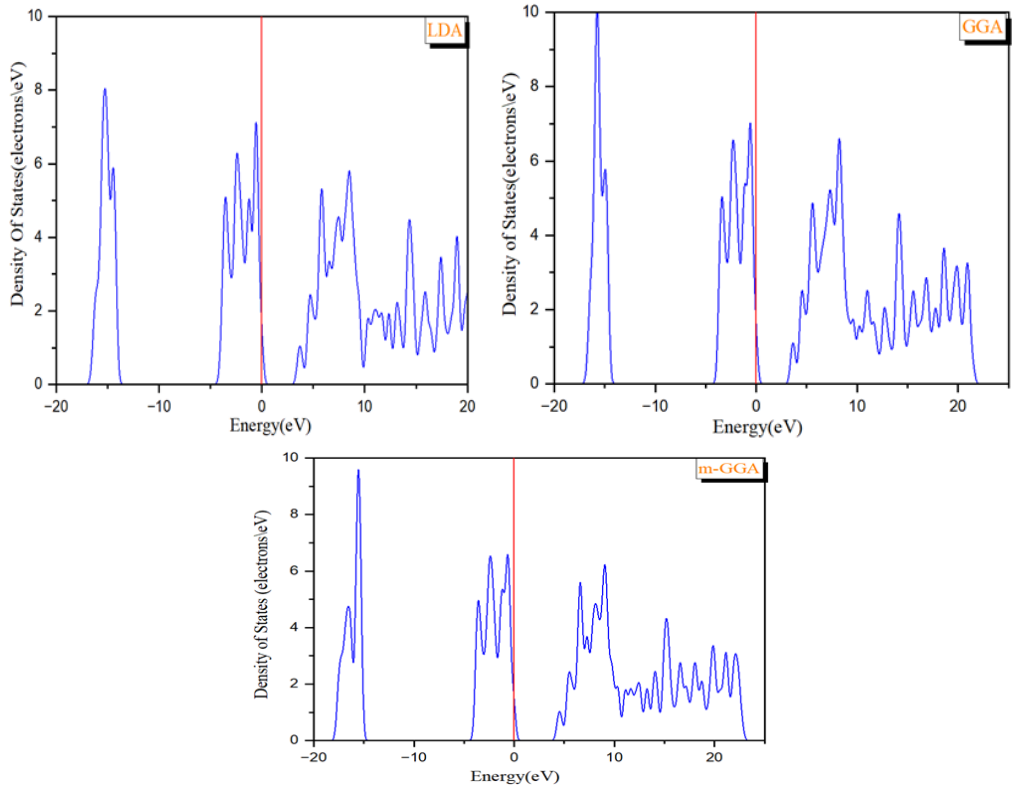


**Figure 3:** The total DOS of Cubic $SrZrO_3$ using Functional LDA, GGA, and M-GGA.

## 3.4 Optical properties

Density functional theory (DFT) is a powerful computational approach for investigating the optical properties of materials, including reflectivity, absorption coefficient, refractive index, and dielectric function. These properties, which are fundamentally linked to the electronic structure, arise from the interaction of the material with electromagnetic radiation. By calculating the frequency-dependent complex dielectric function, $\varepsilon(\omega) = \varepsilon_1(\omega) + i\varepsilon_2(\omega)$, which is derived from interband electronic transitions, DFT enables the accurate estimation of key optical constants (Kohn & Sham, 1965).

### 3.4.1 I Reflectivity

The fraction of light reflected from a material's surface is defined as reflectivity, and it can be calculated from the dielectric function using:

$$R_\omega = \left| \frac{\sqrt{\varepsilon\,(\omega)} - 1}{\sqrt{\varepsilon\,(\omega)} + 1} \right|^2 \tag{1}$$

Although differences in intensity and peak positions are observed, the reflectivity spectra calculated using the three exchange–correlation functionals exhibit similar qualitative features. In all cases, reflectivity begins to increase at approximately 3 eV, reaches a maximum in the low- to mid-energy ultraviolet (UV) region, and then decreases steadily beyond 40 eV. The electronic structure of $SrZrO_3$ gives rise to significant interband transitions, reflected in multiple spectral peaks between 5 and 40 eV. For the LDA functional, reflectivity increases gradually from ∼5 eV and reaches a maximum value of ∼0.47, with distinct peaks observed near 8 eV, 13 eV, and a dominant peak around 26 eV. These features are primarily associated with electronic transitions from O 2p states in the valence band to Zr 4d and Sr 5s states in the conduction band. Above 30 eV, the reflectivity decreases sharply.

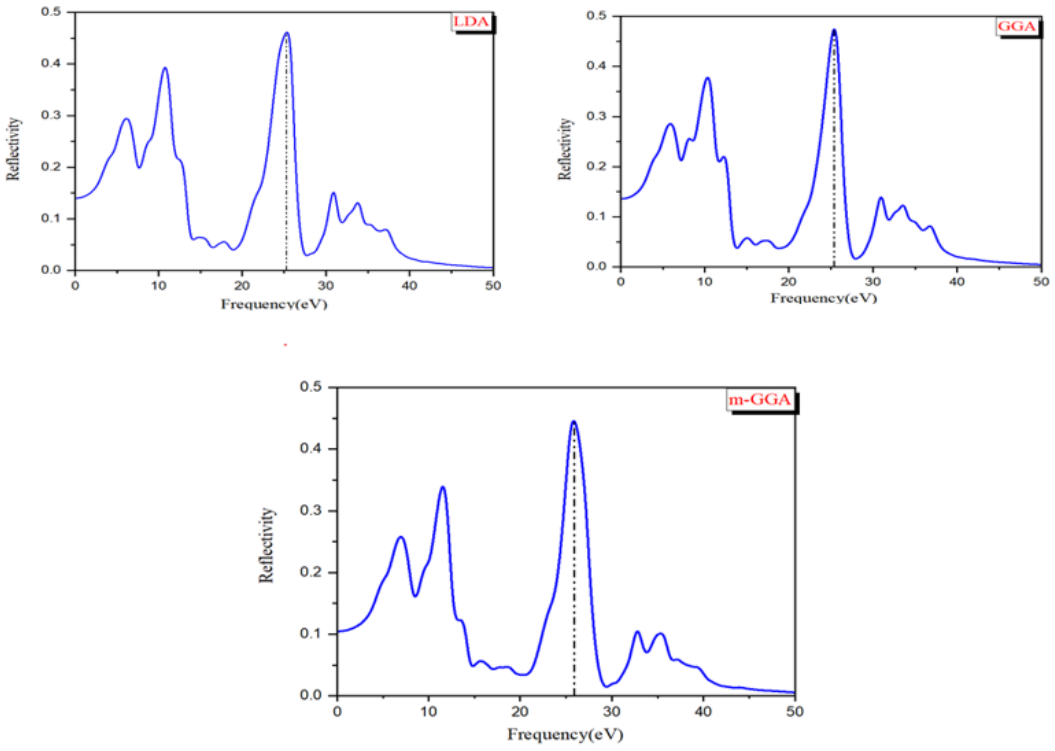


**Figure 4:** Using LDA, GGA, and m-GGA Exchange-Correlation Functional, reflectivity spectra of $SrZrO_3$ are calculated

The GGA spectrum follows a similar overall trend but exhibits slightly red-shifted features and enhanced intensity, particularly for the primary peak near 26 eV. This behavior arises from subtle differences in the predicted band structure, though the overall reflectivity magnitude remains comparable to LDA. The m-GGA functional, owing to its improved treatment of exchange–correlation effects, produces sharper and more intense spectral features. In particular, the strongest peak at ∼26 eV is more pronounced, accompanied by additional fine structures between 30 and 40 eV. Compared to LDA and GGA, the m-GGA spectrum shows better consistency with experimental reflectivity trends reported for wide-bandgap perovskites. The choice of exchange–correlation functional significantly influences the accuracy of the calculated reflectivity spectra: LDA and GGA often underestimate the optical band gap, shifting the reflectivity onset to lower energies, whereas meta-GGA (especially the TB-mBJ potential) provides improved band gap predictions and better agreement with experimental reflectivity profiles, particularly in the UV region. The computed reflectivity spectra of $SrZrO_3$ obtained using LDA, GGA, and m-GGA are illustrated in Figure 4.

### 3.4.2 II Absorption

The absorption coefficient shows the strength of light absorption in a substance. The dielectric function's imaginary element is where it is constructed.

$$\alpha(\omega) = \sqrt{2}\frac{\omega}{c}\left[\sqrt{\varepsilon_1^2(\omega) + \varepsilon_2^2(\omega) - \varepsilon_1(\omega)}\right]^{\frac{1}{2}}$$

The optical absorption behavior of cubic $SrZrO_3$ is closely linked to its electronic structure, particularly the density of states (DOS), which governs the interband transitions responsible for photon absorption. Density Functional Theory (DFT), employing exchange–correlation functionals such as the Local Density Approximation (LDA), Generalized Gradient Approximation (GGA), and meta-Generalized Gradient Approximation (m-GGA), provides an effective framework for investigating these characteristics. Using CASTEP, the effect of the DOS on the absorption spectrum can be systematically analyzed. In $SrZrO_3$, the valence band is primarily composed of O 2p states, while the conduction band is dominated by Zr 4d states. Optical absorption begins when photons excite electrons across the band gap from the valence to the conduction band. Compared with experiment, LDA and GGA tend to underestimate the band gap (∼3.0–3.3 eV), predicting absorption onsets at lower photon energies. By contrast, m-GGA provides improved band gap estimates (∼5.1–5.6 eV) through its inclusion of kinetic energy density, yielding absorption edges in closer agreement with experiment (Cui et al., 2021). Analysis of the total and partial DOS confirms that the sharp rise in absorption above the band gap in the ultraviolet (UV) region originates from strong O 2p → Zr 4d transitions. While LDA and GGA predict this increase at artificially low energies, m-GGA accurately reproduces the onset and magnitude of UV absorption. The calculated absorption coefficient for $SrZrO_3$ indicates significant absorption beginning at ∼4.5–5.5 eV (m-GGA), which increases sharply due to direct allowed transitions at the G–G point of the Brillouin zone (Azeem et al., 2020). Furthermore, the spectra reveal strong absorption above 7 eV, suggesting potential applications of $SrZrO_3$ as a high-k dielectric and UV-blocking material. The improved treatment of exchange–correlation effects within m-GGA produces a more realistic DOS profile and sharper, well-resolved absorption peaks compared with LDA and GGA (Segall et al., 2002). Figure 5 illustrates the calculated absorption spectra of $SrZrO_3$ using LDA, GGA, and m-GGA functionals. Among these, m-GGA provides the most accurate prediction of the absorption edge and peak positions, highlighting its superior capability for modeling the optical properties of wide-bandgap perovskites.

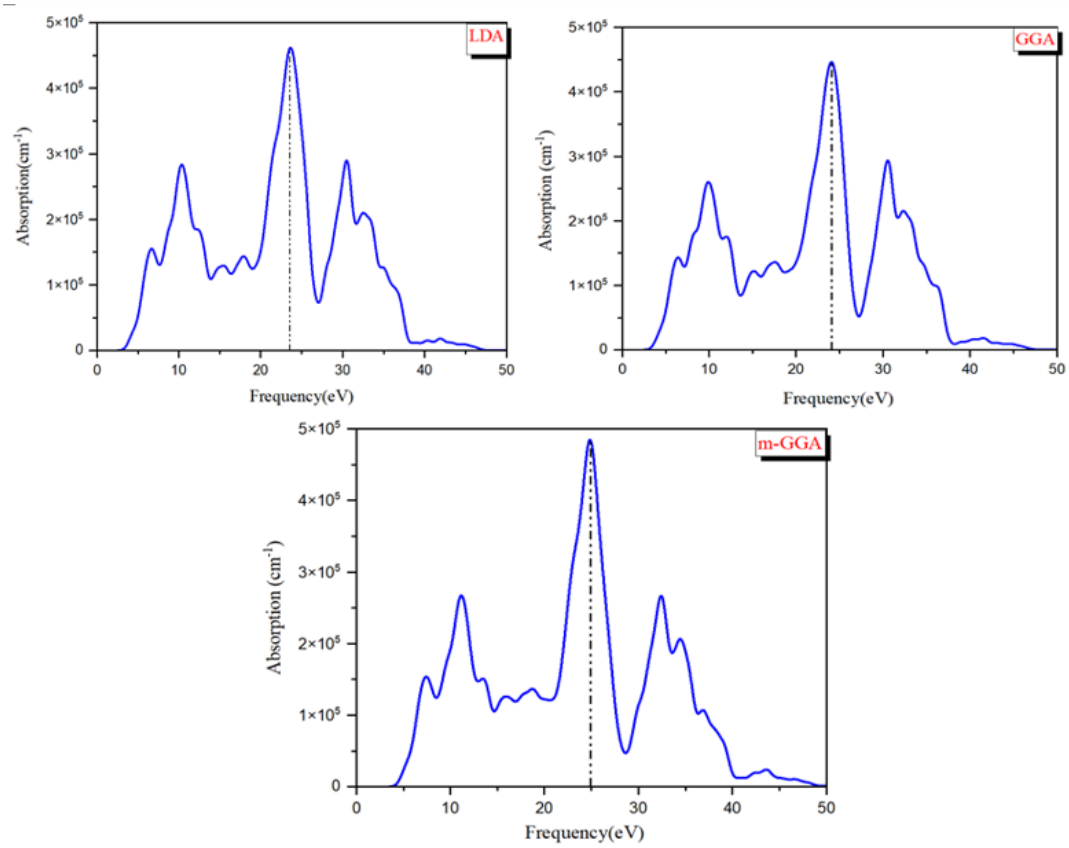


**Figure 5:** Calculated $SrZrO_3$ Absorption Coefficient Spectra Using LDA, GGA, and m-GGA Exchange-Correlation Functional's.

### 3.4.3 III Refractive index

The optical refractive index is a fundamental property that characterizes how light propagates through a material. It is closely related to the dielectric function, and accurate prediction of its values is essential for the design of transparent conductors, optoelectronic devices, and photonic materials. Density Functional Theory (DFT), through the study of the electronic band structure and the frequency-dependent dielectric function, has emerged as a powerful first-principles technique for evaluating the refractive index of solids. The accuracy of these optical property calculations within DFT strongly depends on the choice of exchange–correlation functional. The Local Density Approximation (LDA), which considers only the local electron density, generally underestimates band gaps and consequently tends to overestimate the static refractive index. The Generalized Gradient Approximation (GGA), such as the Perdew–Burke–Ernzerhof (PBE) functional, improves upon LDA by including density gradients; however, it still struggles to provide reliable band-gap predictions for insulators and wide-band-gap materials. By incorporating additional parameters such as kinetic energy density, meta-GGA (m-GGA) functionals, including the Tran–Blaha modified Becke–Johnson (TB-mBJ) potential, yield improved band-gap estimations and consequently more accurate predictions of optical responses. The relationship between the dielectric function and the optical refractive index n($\omega$) is given by:

$$n(\omega) = \sqrt{\frac{|\varepsilon(\omega)| + \varepsilon_1(\omega)}{2}}$$

The real part of the complex dielectric function, denoted as $\varepsilon_1(\omega)$, originates primarily from interband electronic transitions calculated from the Kohn–Sham states (Saifi et al., 2024). Using CASTEP, the optical properties of perovskite $SrZrO_3$ have been investigated within the DFT framework. The static refractive index was reported to be highest with LDA (≈2.57),

intermediate with GGA (≈2.45), and lowest with m-GGA (≈2.32). Among these, the m-GGA value showed the closest agreement with experimental data, highlighting its superior predictive capability. The improved accuracy of m-GGA arises from its enhanced estimation of the band gap and more precise determination of valence and conduction band edges, both of which strongly influence optical transitions. Thus, DFT employing LDA, GGA, and particularly m-GGA functionals provides a reliable basis for refractive index calculations. CASTEP's robust implementation of these functionals enables accurate predictions of optical constants, even for materials with complex electronic structures such as $SrZrO_3$. Notably, m-GGA proves to be the most dependable for reproducing experimental observations. These insights are essential for advancing dielectric engineering, optical coatings, and photonics device design. Figure 6 presents the calculated refractive index spectra of $SrZrO_3$ using the LDA, GGA, and m-GGA functionals.

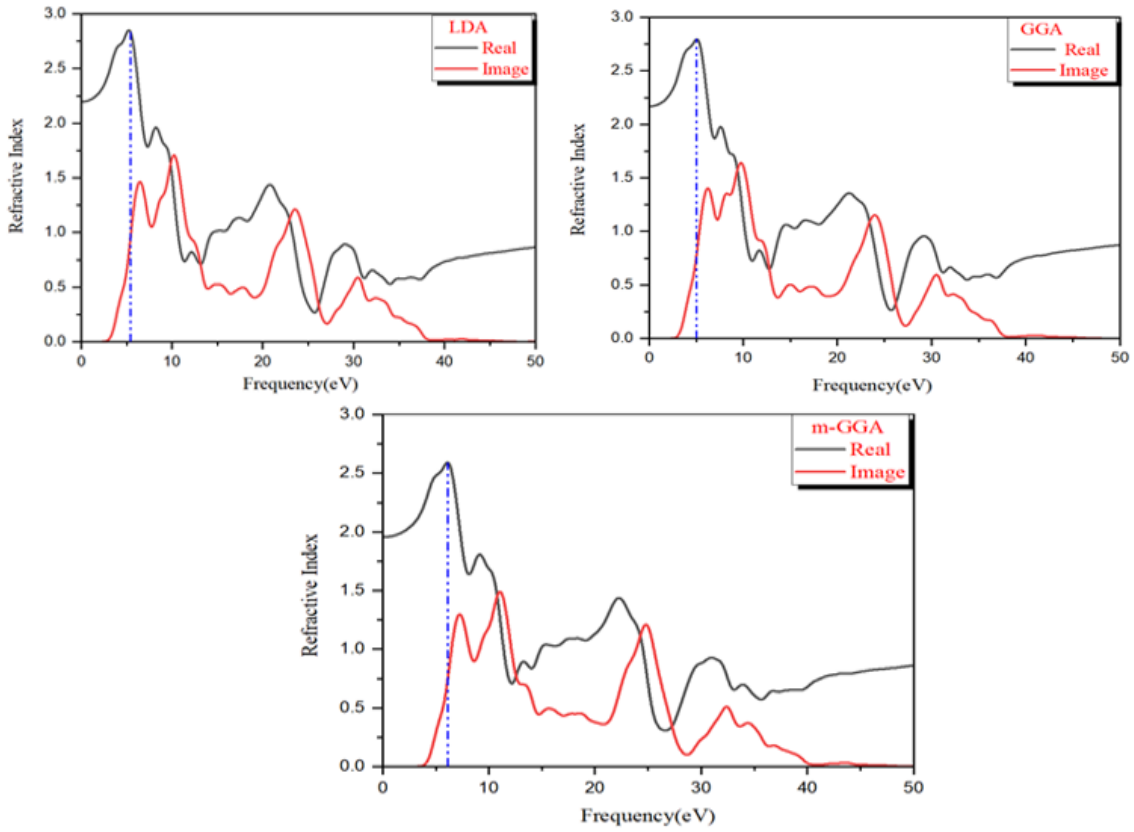


**Figure 6:** Refractive index spectra of $SrZrO_3$ were calculated using exchange-correlation functionals LDA, GGA, and m-GGA.

### 3.4.4 IV Dielectric Function

Density Functional Theory (DFT) provides a robust framework for determining the optical dielectric function of materials such as $SrZrO_3$. The complex dielectric function, expressed as $\varepsilon(\omega) = \varepsilon_1(\omega) + i\varepsilon_2(\omega)$, encapsulates the material's response to electromagnetic radiation, where $\varepsilon_1(\omega)$ describes polarization and dispersion, while $\varepsilon_2(\omega)$ reflects absorption arising from interband electronic transitions. The accuracy of the calculated dielectric function strongly depends on the choice of exchange–correlation functional employed in DFT. The Local Density Approximation (LDA), which assumes a uniform electron density, generally yields reliable structural properties but underestimates the band gap. This results in an overestimation of the static dielectric constant and shifts the absorption edge in $\varepsilon_2(\omega)$ toward lower energies for $SrZrO_3$. The Generalized Gradient Approximation (GGA), such as the widely applied Perdew–Burke–

Ernzerhof (PBE) functional, improves upon LDA by incorporating electron density gradients. For $SrZrO_3$, GGA provides a slightly more accurate band-gap prediction and, consequently, a more realistic dielectric response; however, it often fails to precisely reproduce the detailed spectral features, particularly the exact positions of $\varepsilon_2(\omega)$ peaks. Meta-GGA (m-GGA) functionals, including the Tran–Blaha modified Becke–Johnson (TB-mBJ) potential, extend accuracy further by incorporating kinetic energy density. This enhancement leads to more precise band-gap predictions and improved descriptions of the electronic structure, thereby yielding more accurate dielectric function spectra. Recent DFT studies using m-GGA within CASTEP demonstrated reduced overestimation of the static dielectric constant compared to LDA and GGA, along with closer agreement between theoretical and experimental values of $\varepsilon_1(0)$ and interband transition peaks in $\varepsilon_2(\omega)$ (Bouzaid et al., 2024). Overall, while LDA and GGA provide qualitative insights into the dielectric response of $SrZrO_3$, m-GGA delivers quantitatively superior predictions, capturing both the onset of absorption and the correct magnitudes of the real and imaginary dielectric components. These findings establish m-GGA as the most reliable functional for theoretical investigations of complex oxide systems. Consequently, DFT—especially when combined with advanced functionals such as m-GGA—offers a comprehensive approach for exploring the optical dielectric function of $SrZrO_3$, thereby deepening our understanding of its light–matter interactions and enhancing its potential for photonic and optoelectronic applications.

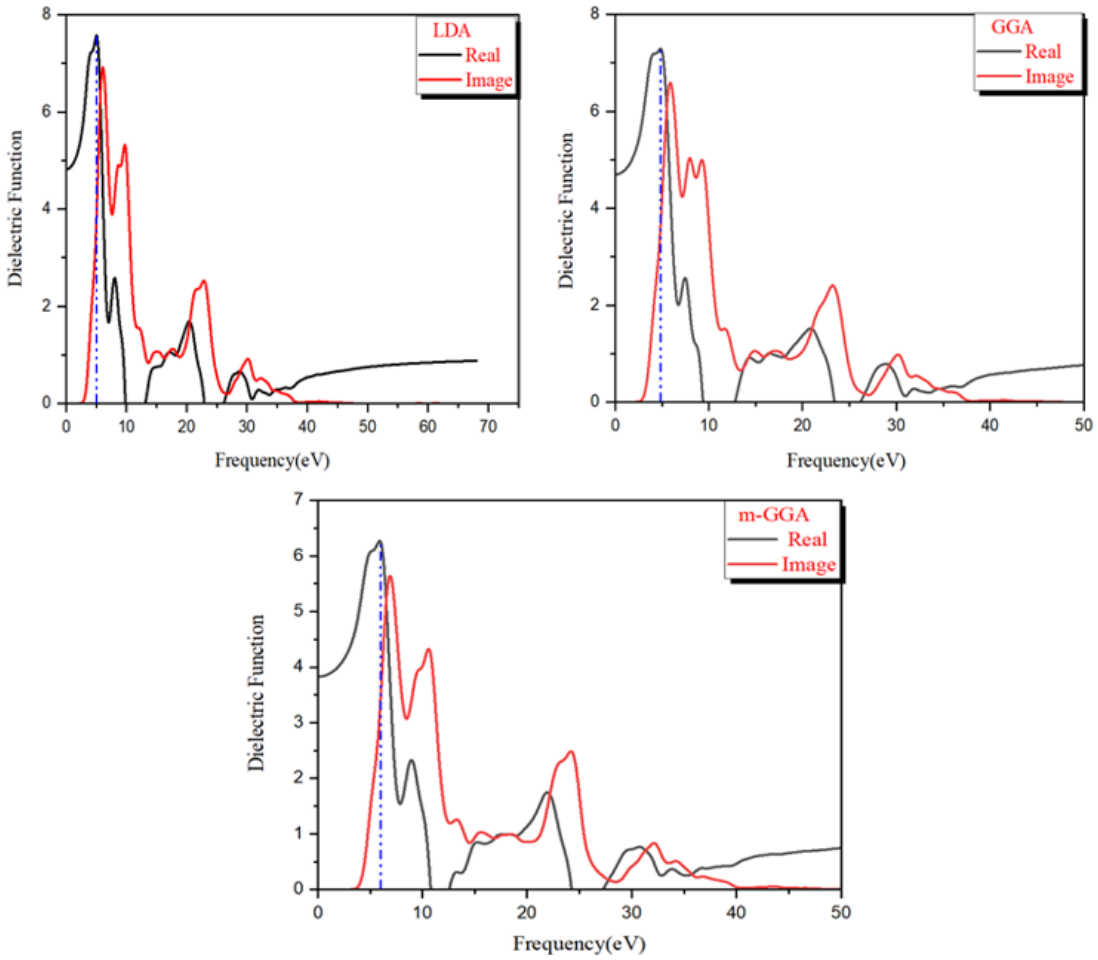


**Figure 7:** The Dielectric Function of $SrZrO_3$: Real and Imaginary Parts Calculated Using LDA, GGA, and m-GGA Exchange-Correlation Functionals.

### 3.5 Mulliken Charge Analysis

The Mulliken charge distribution of $SrZrO_3$, calculated using different density functional theory (DFT) functionals (LDA, GGA, and m-GGA), reveals significant variations in electron distribution among Zr, Sr, and O atoms. For oxygen (O), LDA and GGA predict negative charges ranging from 0.76e to –0.79 e, reflecting its electron-rich character. In contrast, m-GGA projects a more substantial negative charge of –0.85e, indicating higher electron density on oxygen. The total electron population on O is correspondingly larger in m GGA (3.42e) than in LDA/GGA (3.38–3.40 e), likely due to the inclusion of higher-order exchange–correlation effects. Additionally, the p-orbital occupancy on O increases from ∼2.47–2.48e (LDA/GGA) to 2.50 e (m-GGA), consistent with enhanced covalent character in the bonding. Zirconium (Zr) exhibits a positive Mulliken charge, confirming electron transfer from Zr to O. The charge on Zr increases from +1.03e (LDA) to +1.08e (GGA) and +1.15e (m-GGA), while the total electron population varies from 5.49e (LDA) to 5.43e (m-GGA). These changes suggest that m-GGA captures additional electron density contributions, likely due to hybridization effects. The d-orbital occupancy of Zr decreases slightly from 1.04e (LDA) to 1.02e (GGA) and 0.96e (m-GGA), reflecting enhanced Zr–O bonding characteristics under m-GGA.Strontium (Sr) demonstrates electron-donating behavior while maintaining a positive charge. The Mulliken charge on Sr increases slightly from +1.26e (LDA) to +1.30e (GGA), then decreases to +1.39e (m-GGA), while the total electron population rises to 4.30e (m-GGA) from 4.37e (LDA). Small increases in the p-orbital occupancy across functionals, with m-GGA predicting 3.02e (identical to LDA/GGA), suggest a more polar bonding environment. Overall, these results indicate that m-GGA provides a more accurate description of the electronic distribution and bonding in $SrZrO_3$, in agreement with previous studies (Eglitis, 2012).

**Table 3:** Using LDA, GGA, and M-GGA, the orbital charges (electron), total charge, and anatomic Mulliken charge (electron) of $SZrO_3$.

| Methods | Species | s | p | d | F | Total | Mulliken Charge (e) |
|---|---|---|---|---|---|---|---|
| LDA | O | 0.91 | 2.47 | 0.00 | 0.00 | 3.38 | -0.76 |
| | O | 0.91 | 2.47 | 0.00 | 0.00 | 3.38 | -0.76 |
| | O | 0.91 | 2.47 | 0.00 | 0.00 | 3.38 | -0.76 |
| | Sr | 1.06 | 3.02 | 0.29 | 0.00 | 4.37 | 1.26 |
| | Zr | 1.18 | 3.26 | 1.04 | 0.00 | 5.49 | 1.03 |
| GGA | O | 0.92 | 2.48 | 0.00 | 0.00 | 3.40 | -0.79 |
| | O | 0.92 | 2.48 | 0.00 | 0.00 | 3.40 | -0.79 |
| | O | 0.92 | 2.48 | 0.00 | 0.00 | 3.40 | -0.79 |
| | Sr | 1.06 | 3.02 | 0.27 | 0.00 | 4.35 | 1.30 |
| | Zr | 1.18 | 3.26 | 1.02 | 0.00 | 5.46 | 1.08 |
| m-GGA | O | 0.92 | 2.50 | 0.00 | 0.00 | 3.42 | -0.85 |
| | O | 0.92 | 2.50 | 0.00 | 0.00 | 3.42 | -0.85 |
| | O | 0.92 | 2.50 | 0.00 | 0.00 | 3.42 | -0.85 |
| | Sr | 1.03 | 3.02 | 0.26 | 0.00 | 4.30 | 1.39 |
| | Zr | 1.16 | 3.31 | 0.96 | 0.00 | 5.43 | 1.15 |

### 3.6 Bond Length and Population Analysis

The structural properties of cubic $SrZrO_3$ (perovskite structure) were calculated using three exchange–correlation functionals: LDA, GGA, and meta-GGA (m-GGA). This analysis focuses on the bond lengths and populations of Zr–O, Sr–O, and O–O interactions. Due to LDA's tendency to overbind atoms, it typically predicts the shortest Zr–O bond lengths. In contrast, GGA and m-GGA yield slightly longer bond lengths that are in closer agreement with experimental values (2.065–2.093 Å) (Alay-e-Abbas et al., 2019). Across all functionals, the Zr–O bond populations indicate significant covalent character, with GGA predicting the largest value (0.86). As expected from the 12-fold coordination of Sr in the A-site of the perovskite structure, the Sr–O bond lengths are substantially longer than the Zr–O bonds. Both GGA and

m-GGA slightly overestimate these distances compared to LDA. The relatively low bond populations (∼0.10–0.14) suggest that Sr–O bonds are predominantly ionic. Experimentally, at room temperature, the Zr–O and Sr–O bond lengths are approximately 2.065 A° and 2.92–2.96 A°, respectively. While LDA underestimates both Zr–O and Sr–O distances, consistent with its known contraction tendency, the GGA and m-GGA results closely match the experimental data, demonstrating their improved accuracy in describing the structural properties of $SrZrO_3$.

**Table 4:** Show the bond overlap populations and bond lengths (Å) for $SrZrO_3$ that have been calculated using LDA, GGA, and M-GGA.

| Methods | Bond | Population | Length (Å) |
|---|---|---|---|
| LDA | Zr–O | 0.84 | 2.05898 |
| | Sr–O | 0.15 | 2.91184 |
| | O–O | -0.10 | 2.91184 |
| GGA | Zr–O | 0.86 | 2.09322 |
| | Sr–O | 0.14 | 2.96026 |
| | O–O | -0.09 | 2.96026 |
| m-GGA | Zr–O | 0.91 | 2.06540 |
| | Sr–O | 0.10 | 2.92092 |
| | O–O | -0.09 | 2.92092 |

# 4 Conclusion

In this study, the structural, electronic, optical, and bonding properties of $SrZrO_3$ were systematically investigated using first-principles calculations within the frameworks of LDA, GGA, and m-GGA exchange–correlation functionals. The calculated lattice parameters indicate that m-GGA provides the most accurate results, closely matching experimental data, whereas LDA tends to underestimate and GGA tends to overestimate the experimental values. Bond length and bond population analyses reveal that Sr–O bonds are predominantly ionic, while Zr–O bonds exhibit mixed ionic–covalent character. Mulliken charge analysis further supports this conclusion, showing partial electron transfer from Sr and Zr atoms to O atoms. Electronic band structure and density of states (DOS) analyses confirm that $SrZrO_3$ is an indirect band gap semiconductor. As expected, m-GGA slightly corrects the underestimation of the band gap observed in LDA and GGA, providing a value closer to the experimental band gap (∼3.75 eV). Consistent with previous theoretical and experimental studies, the conduction band is mainly composed of Zr 4d states, while the valence band is dominated by O 2p states. Regarding optical properties, the absorption spectra indicate that m-GGA better reproduces the experimental optical transitions, with absorption onsets corresponding to the expected band gap energies. Reflectivity and refractive index spectra exhibit typical wide-band-gap perovskite behavior, with minor variations depending on the functional employed. Dielectric function calculations demonstrate a high static dielectric constant, confirming the material's potential for optoelectronic and dielectric applications. Overall, across all properties investigated, the m-GGA functional provides the best agreement with experimental data, establishing it as a reliable approach for predicting the physical properties of $SrZrO_3$.

# References

Alay-e-Abbas, S.M., Yousaf, M.W., Abbas, G., Amin, N., & Laref, A. (2019). Theoretical investigation of thermodynamic and optoelectronic properties of Ce4+ doped SrZrO3 ceramics: a DFT study. *Ceramics International, 45*(15), 18281-18290.

Azeem, W., Luo, C.Q., Xu, C., Zhou, S., Wagner, A., Butterling, M., ... & Ling, F.C.C. (2020). Ferromagnetism in undoped ZnO grown by pulsed laser deposition. *Materials Research Express, 7*(5), 056102.

Bouzaid, A., Ziat, Y., Belkhanchi, H., Hamdani, H., Koufi, A., Miri, M., ... & Zarhri, Z. (2024). Ab initio study of the structural, electronic, and optical properties of MgTiO3 perovskite materials doped with N and P. In *E3S Web of Conferences* (Vol. 582, p. 02006). EDP Sciences.

Colomban, P. (Ed.). (1992). *Proton Conductors: Solids, membranes and gels-materials and devices* (No. 2). Cambridge University Press.

Celik, G., Cabuk, S. (2013). First-principles study of electronic structure and optical properties of Sr (Ti, Zr) O3. *Central European Journal of Physics, 11*(3), 387-393.

Chakraborti, S., Rahaman, S.M., Alam, M.N., Mandal, A., Ghosh, B., Dey, K., & Chakraborti, T. (2015). Na+/K+-ATPase: a perspective. In *Regulation of Membrane Na+-K+ ATPase* (pp. 3-30). Cham: Springer International Publishing.

Cui, Y.H., Guo, M.Y., Shao, Y.X., Yang, Y., Ma, Y.D., Sun, W.W., ... & Yan, D.R. (2021). Effects of SiC on microstructure and properties of plasma sprayed ZrB2–ZrC composite coating. *Ceramics International, 47*(9), 12753-12761.

Davies, R.A., Islam, M.S., & Gale, J.D. (1999). Dopant and proton incorporation in perovskite-type zirconates. *Solid State Ionics, 126*(3-4), 323-335.

Eglitis, R.I. (2013). Ab initio calculations of the atomic and electronic structure of BaZrO3 (111) surfaces. *Solid State Ionics*, 230, 43-47.

Feng, Z., Hu, H., Cui, S., & Bai, C. (2008). First-principles study of optical properties of SrZrO3 in cubic phase. *Solid state communications, 148*(9-10), 472-475.

Fukatsu, N., Kurita, N., Yajima, T., Koide, K., & Ohashi, T. (1995). Proton conductors of oxide and their application to research into metal-hydrogen systems. *Journal of Alloys and Compounds, 231*(1-2), 706-712.

Galicka-Fau, K., Legros, C., Andrieux, M., Herbst-Ghysel, M., Gallet, I., Condat, M., ... & Servet, B. (2008). Thickness determination of SrZrO3 thin films using both X-ray reflectometry and SIMS techniques. *Thin Solid Films, 516*(22), 7967-7973.

Ghaleb, A.M., Ahmed, A.Q. (2022). Structural, electronic, and optical properties of sphalerite ZnS compounds calculated using density functional theory (DFT). *Chalcogenide Letters, 19*(5).

Ghaleb, A.M., Shihatha, A.T., & Ghaleb, Z.T. (2022). Investigation of the physical properties and Mulliken charge distribution of the cube perovskite BiGaO 3 is calculated by GGA-PBE. *Digest Journal of Nanomaterials & Biostructures (DJNB), 17*(4).

Iwahara, H., Yajima, T., Hibino, T., & Ushida, H. (1993). Performance of Solid Oxide Fuel Cell Using Proton and Oxide Ion Mixed Conductors Based on $BaCe1-xSmxO3-\alpha$. *Journal of the Electrochemical Society, 140*(6), 1687.

Kennedy, B.J., Howard, C.J., & Chakoumakos, B.C. (1999). High-temperature phase transitions in SrZrO 3. *Physical Review B, 59*(6), 4023.

Kirci, O., Pandir, Y., Latifa, A., & Bulut, H. (2024). A new version of trial equation method for a complex nonlinear system arising in optical fibers. *Optical and Quantum Electronics, 56*(6), 1019.

Kohn, W., Sham, L.J. (1965). Self-consistent equations including exchange and correlation effects. *Physical review, 140*(4A), A1133.

Ling, H.Q., Li, A.D., Wu, D., Tang, Y.F., Liu, Z.G., & Ming, N.B. (2002). Fabrication and characterization of SrZrO3 thin films prepared by sol–gel. *Materials chemistry and physics, 75*(1-3), 170-173.

Lindan, P.J., Probert, M.J., Segall, M.D., Pickard, C.J., Hasnip, P., Clark, S.J., & Payne, M.C. (2002). First-principles simulation: ideas, illustrations and the CASTEP code. *Journal of Physics: Condensed Matter, 14*(11), 2717-2744.

Marana, N.L., Longo, V.M., Longo, E., Martins, J.B.L., & Sambrano, J.R. (2008). Electronic and structural properties of the (1010) and (1120) ZnO surfaces. *The Journal of Physical Chemistry A, 112*(38), 8958-8963.

Mete, E., Shaltaf, R., & Ellialtıoğlu, Ş. (2003). Electronic and structural properties of a 4 d perovskite: cubic phase of SrZrO 3. *Physical Review B, 68*(3), 035119.

Moreira, M.L., Andres, J., Longo, V.M., Li, M.S., Varela, J.A., & Longo, E. (2009). Photoluminescent behavior of SrZrO3/SrTiO3 multilayer thin films. *Chemical Physics Letters, 473*(4-6), 293-298.

Muscat, J., Wander, A., & Harrison, N.M. (2001). On the prediction of band gaps from hybrid functional theory. *Chemical Physics Letters, 342*(3-4), 397-401.

Perdew, J.P., Burke, K., & Ernzerhof, M. (1996). Generalized gradient approximation made simple. *Physical review letters, 77*(18), 3865.

Park, H.S., Kim, D.H., Kim, S.J., & Lee, K.S. (2006). The photocatalytic activity of 2.5 wt Cu-doped TiO2 nano powders synthesized by mechanical alloying. *Journal of Alloys and Compounds, 415*(1-2), 51-55.

Perdew, J.P., Zunger, A. (1981). Self-interaction correction to density-functional approximations for many-electron systems. *Physical review B, 23*(10), 5048.

Perdew, J.P. (1997). Generalized gradient approximation made simple. *Phys. Rev. Lett.*, 77, 3868.

Shein, I.R., Shein, K.I., & Ivanovskii, A.L. (2007). Elastic and electronic properties and stability of SrThO3, SrZrO3 and ThO2 from first principles. *Journal of nuclear materials, 361*(1), 69-77.

Saifi, F., Anas, S.M., Tahzeeb, R., Shariq, M., & Alam, M. (2024). Numerical investigation of blast loading effects on a thin-walled cylindrical steel storage tank. *Materials Today: Proceedings.*

Souptel, D., Behr, G., & Balbashov, A.M. (2002). SrZrO3 single crystal growth by floating zone technique with radiation heating. *Journal of Crystal Growth, 236*(4), 583-588.

Sambrano, J.R., Nobrega, G.F., Taft, C.A., Andres, J., & Beltran, A. (2005). A theoretical analysis of the TiO2/Sn doped (1 1 0) surface properties. *Surface Science, 580*(1-3), 71-79.

Sambrano, J.R., Nobrega, G.F., Taft, C.A., Andres, J., & Beltran, A. (2005). A theoretical analysis of the TiO2/Sn doped (1 1 0) surface properties. *Surface Science, 580*(1-3), 71-79.

Shende, R.V., Krueger, D.S., Rossetti, G.A., & Lombardo, S.J. (2001). Strontium zirconate and strontium titanate ceramics for high-voltage applications: synthesis, processing, and dielectric properties. *Journal of the American Ceramic Society, 84*(7), 1648-1650.

Smith, A.J., Welch, A.J.E. (1960). Some mixed metal oxides of perovskite structure. *Acta Crystallographica, 13*(8), 653-656.

Tsai, C.C., Teng, H. (2008). Chromium-doped titanium dioxide thin-film photoanodes in visible-light-induced water cleavage. *Applied Surface Science, 254*(15), 4912-4918.

Tran, F., Blaha, P. (2009). Accurate band gaps of semiconductors and insulators¡? format?¿ with a semilocal exchange-correlation potential. *Physical review letters, 102*(22), 226401.

Vali, R. (2008). Band structure and dielectric properties of orthorhombic $SrZrO_3$. *Solid State Communications, 145*(9-10), 497-501.

Wu, Z.H., Liu, H.X., Cao, M.H., Shen, Z.Y., Yao, Z.H., Hao, H., & Luo, D.B. (2008). Effect of BaO-Al2O3-B2O3-SiO2 glass additive on densification and dielectric properties of Ba0. 3Sr0. 7TiO3 ceramics. *Journal of the Ceramic Society of Japan, 116*(1350), 345-349.

Yajima, T., Suzuki, H., Yogo, T., & Iwahara, H. (1992). Protonic conduction in SrZrO sub 3-based oxides. *Solid State Ionics;(Netherlands), 51*(1/2).

Yu, T., Zhu, W.G., Chen, C.H., Chen, X.F., & Krishnan, R.G. (2004). Preparation and characterization of sol–gel derived CaZrO3 dielectric thin films for high-k applications. *Physica B: Condensed Matter, 348*(1-4), 440-445.

Zhao, X., Vanderbilt, D. (2002). First-principles study of structural, vibrational, and lattice dielectric properties of hafnium oxide. *Physical Review B, 65*(23), 233106.